Artesunate Differentially Attenuates STZ-Induced Alzheimer-Like Pathology in Young and Old Mice by Targeting the Hippocampal Ferroptosis-Autophagy-Mitochondrial Redox Axis

Chengchen REN[1], Mudasir AHMAD[2], Chun XIAO[3]

[1]Department of Neurosurgery, Jinan Third People's Hospital, Jinan, China, [2]Department of Clinical Biochemistry, University of Kasmir, Srinagar, Jammu and Kashmir, India, [3]Department of Neurosurgery, The First Affiliated Hospital of Chongqing Medical and Pharmaceutical College, Chongqing, China

Received February 26, 2026
Accepted July 14, 2026

Summary

Aging is a critical determinant of Alzheimer disease (AD) susceptibility and therapeutic responsiveness. The current study aimed to evaluate the effect of artesunate on attenuating streptozotocin (STZ)-induced Alzheimer-like pathology by modulating the ferroptosis-autophagy-mitochondrial redox axis. STZ-induced AD-like pathology was established in young and old mice, which were divided into control, AD, and AD + artesunate groups. Cognitive function was measured with the Morris Water Maze (MWM) test to evaluate spatial learning and memory and using the novel object recognition (NOR) test to assess recognition memory. Protein expression levels of ferroptosis-related proteins (GPX4, SLC7A11, and ACSL4), autophagy proteins (LC3-I/II, Beclin-1, and p62), mitochondrial redox homeostasis and antioxidant defense proteins (SOD2 and HO-1), and synaptic integrity (PSD95 and synaptophysin) were evaluated. Artesunate significantly enhanced learning and memory in young AD mice, as evidenced by reduced escape latency and increased time spent in the target quadrant in the MWM, as well as a higher discrimination index in the NOR test. These behavioral improvements were associated with restored expression of GPX4 and SLC7A11 and suppression of ACSL4. These molecular changes were accompanied by a significant reduction in MDA and 4-HNE levels, enhanced autophagic flux (increased LC3-II/LC3-I ratio and Beclin-1 expression), and restoration of SOD2 and HO-1 levels. Moreover, artesunate reinstated synaptic integrity, as evidenced by increased expression of PSD95 and synaptophysin. Older AD mice showed slight cognitive recovery after artesunate administration, and exhibited poor performance in the MWM and NOR tests. Although targeting the ferroptosis-autophagy-mitochondrial redox axis represents a promising therapeutic strategy, aging significantly reduces molecular responsiveness and decreases treatment efficacy in AD.

Key words

Artesunate • Alzheimer disease • Ferroptosis • Autophagy • Mitochondrial redox

Corresponding author

C. Xiao, Department of Neurosurgery, The First Affiliated Hospital of Chongqing Medical and Pharmaceutical College, Chongqing, 400060, China. E-mail: xc98700190@outlook.com

Introduction

Alzheimer disease (AD) is a multidimensional neurodegenerative disorder that is characterized by cognitive impairment, synaptic dysfunction, and selective neuron degeneration [1]. Even though amyloid-β deposition and tau hyperphosphorylation are still pathological hallmarks, there is growing evidence that disrupted cellular redox homeostasis, mitochondrial integrity, and regulated cell death pathways are the primary drivers of disease progression, especially in sporadic, late-onset AD [2,3]. The most common risk factor of AD is aging, which drastically changes all these interconnected pathways and makes the aged brain susceptible to oxidative damage and less responsive to therapeutic intervention [4].

 An open access article under the CC BY 4.0 license https://creativecommons.org/licenses/by/4.0/ © 2026 by the authors. Published by the Institute of Physiology, Czech Academy of Sciences, Prague, Czech Republic. E-mail: physres@fgu.cas.cz, www.biomed.cas.cz/physiolres

Mitochondrial dysfunction is a chronic and early event in AD pathology that occurs before the development of plaques and tangles [5]. The dysfunction of the electron transport chain, decreased antioxidant capacity of mitochondria, and overproduction of reactive oxygen species (ROS) stimulate the oxidative injury of lipids, proteins, and nucleic acids [6]. The lipid peroxidation process is particularly harmful to the brain as it is rich in polyunsaturated fatty acids, which eventually affect the integrity of the membrane, synaptic signaling, and neuronal survival [7]. It is important to note that aging increases the redox dysfunction of mitochondria by inhibiting the activity of antioxidant enzymes including superoxide dismutase 2 (SOD2) and heme oxygenase-1 (HO-1), which enhances susceptibility to oxidative stress [8].

Ferroptosis is one of the emerging cell death mechanisms that have been implicated in the pathogenesis of AD [9]. Ferroptosis is an iron-dependent, non-apoptotic type of regulated cell death characterized by uncontrolled lipid peroxidation and breakdown of the glutathione-dependent antioxidant [10]. The basic molecular regulators of ferroptosis, such as glutathione peroxidase 4 (GPX4), cystine/glutamate antiporter SLC7A11, and acyl-CoA synthetase long-chain family member 4 (ACSL4), have been reported to be dysregulated in AD brains and experimental animal models [11] [12]. Depletion of GPX4 function or decrease of cystine uptake *via* SLC7A11 restricts the availability of glutathione, thereby inhibiting the detoxification of lipid hydroperoxides, whereas polyunsaturated fatty acids are incorporated into phospholipids by ACSL4, making membranes susceptible to peroxidative damage [13] [14]. There is mounting evidence that ferroptosis is involved in the pathogenesis of AD with regard to synaptic degeneration, neuronal loss, and cognitive impairment [15].

Autophagy is a vital cellular quality control process, which ensures neuronal homeostasis by damaged organelles, oxidized lipids, and misfolded proteins [16]. Malfunctioning autophagic flux is a characteristic feature of AD, which is also enhanced by age and results in the accumulation of malfunctioning mitochondria as well as oxidative products [17]. Notably, autophagy is mechanistically linked with ferroptosis by controlling cellular iron levels, lipid metabolism, and antioxidant response [18]. Induced ferritinophagy and other forms of autophagic processes can elevate the labile iron pools, which enhances ferroptotic signaling, and autophagy defects inhibit the ability of cells to clear oxidative damage [19]. Therefore, impairment of the ferroptosis-autophagy axis leads to a feed-forward mechanism of mitochondrial malfunction and lipid peroxidation that promotes neurodegeneration [20].

The AD-like model induced by streptozotocin (STZ) reproduces the main characteristics of sporadic AD, such as brain insulin resistance, mitochondrial dysfunction, oxidative stress, synaptic loss, and cognitive impairment [21]. Notably, the pathology caused by STZ is closely related to increased lipid peroxidation, impaired antioxidant defenses, and dysregulated autophagy, which is why it is a valid model to study redox- and ferroptosis-targeted therapeutic options in various age groups [22].

Artesunate is a semi-synthetic derivative of artemisinin and a clinically approved antimalarial drug that has become a pleiotropic regulator of redox signaling, autophagy, and regulated cell death [23]. In addition to its known antiparasitic effect, artesunate has strong antioxidant, anti-inflammatory, and cytoprotective potentials in various disease models [24]. Artesunate has been demonstrated to regulate ferroptosis by maintaining the activity of GPX4, iron homeostasis, and inhibiting lipid peroxidation [25]. Moreover, artesunate can promote autophagic flux and recover redox balance in mitochondria, which may imply its ability to disrupt the pathogenic ferroptosis-autophagy-mitochondrial axis, which underlies AD progression [26].

Importantly, to the best of our knowledge, this is the first study to directly compare the neuroprotective effects of artesunate in young versus aged STZ-induced Alzheimer-like mice, thereby addressing whether aging modulates the responsiveness of the ferroptosis-autophagy-mitochondrial redox axis to pharmacological intervention.

Nevertheless, the process of aging results in radical changes in cellular responses to stress, such as decreased efficiency of autophagic processes, decreased mitochondrial resistance, disrupted iron metabolism, and disturbed redox signaling [8]. This is because these age-related changes can greatly compromise the neuroprotective properties of artesunate, which has not been actively investigated. The way in which aging modulates the molecular responsiveness of ferroptosis, autophagy and mitochondrial antioxidant systems to pharmacological therapy is important to translate neuroprotective findings into clinical therapies.

This paper examined the effects of artesunate on STZ-induced AD-like pathology in young and old mice.

We particularly focused on the question of whether artesunate selectively regulates the ferroptosis-autophagy-mitochondrial redox axis, and the relationship between the molecular alterations and cognitive performance and synapses. Through a combination of behavioral studies and molecular and biochemical measurements, this study offers a mechanistic understanding of how aging limits therapeutic responsiveness and ferroptosis-autophagy crosstalk as a potential promising, but age-sensitive, therapeutic target in Alzheimer disease.

Materials and Methods

Animals and ethical approval

Male C57BL/6J mice were obtained from a certified animal facility and kept in pathogen-free conditions. The study was conducted using two age groups: young (3-4 months old; 25-30 g) and old mice (18-20 months old; 32-40 g). Animals were kept under controlled environmental conditions (12 h light/dark cycle, temperature 22±2 °C, humidity 50-60 % and ad libitum access to normal chow and water). The Laboratory Animal Ethics Committee, West China Hospital, Sichuan University (Ethics Approval No. 20251126017) approved all the experimental procedures, and the study followed the guidelines of the National Institutes of Health (NIH) on the care and use of laboratory animals. The reporting and the study design were in accordance with the ARRIVE guidelines. All efforts were made to minimize animal suffering and reduce the number of animals used.

Randomization, experimental design, and blinding

Mice were randomly placed in experimental groups (n=10 mice per group unless otherwise specified) based on computerized random number generator into the following age groups per age cohort:

- Control group (vehicle-treated)
- STZ-induced AD group
- STZ + Artesunate-treated group

Blinding was performed by ensuring that investigators conducting behavioral testing, tissue processing, biochemical assays, and data analysis were unaware of the treatment group assignments. A priori power analysis indicated a minimum detectable effect size of 20 %, with 80 % statistical power at α=0.05, which was used to determine sample size.

Induction of sporadic Alzheimer-like pathology

Streptozotocin (STZ) was administered intracerebroventricularly (ICV) to induce AD-like pathology in mice, which is a validated model of sporadic AD that is associated with brain insulin resistance, oxidative stress, loss of synapses, and cognitive impairment.

Ketamine (100 mg/kg) and xylazine (10 mg/kg) were used to anesthetize mice and position them in a stereotaxic apparatus. STZ was dissolved in cold citrate buffer (0.05 M, pH 4.5) and injected bilaterally into the lateral ventricles at the dosage of 3 mg/kg, administered in two instances on day 1 and day 3. Relative to bregma, stereotaxic coordinates were anteroposterior -0.3 mm, mediolateral ±1.0 mm, dorsoventral -2.5 mm. The volume of each injection was 2 µl at 0.5 µl/min. An additional 2 min was allowed for the needle to remain in place to avoid backflow. Equivalent amounts of citrate buffer were administered to control animals.

Artesunate treatment

Artesunate (≥98 % purity) was dissolved in dimethyl sulfoxide (DMSO) and then diluted in sterile saline to a final DMSO concentration of less than 0.1 %. Artesunate was given at the dosage of 30 mg/kg/day intraperitoneally for 21 consecutive days starting 7 days after the last STZ injection to enable development of the AD-like pathology. The dose and treatment duration were chosen according to the published studies that showed effective redox signaling, autophagy, and ferroptosis modulation without any systemic toxicity. The STZ-only and control groups were given the same volume of vehicle.

Following a 7-day interval after the final STZ injection, artesunate treatment was initiated on day 10 and continued daily until day 30. Behavioral assessments evaluating learning, memory, and cognitive function were conducted during the final week of the treatment period. Upon completion of behavioral testing, mice were euthanized, and brain tissues were harvested for subsequent biochemical, molecular, and histopathological analyses.

Chloroquine treatment

To assess autophagic flux *in vivo*, a subset of mice (n=5 per group) from each experimental group received chloroquine (CQ), a lysosomal inhibitor that blocks autophagosome-lysosome fusion and prevents lysosomal degradation of autophagic cargo. Chloroquine was administered intraperitoneally at a dose of 50 mg/kg

4 h prior to euthanasia. Following treatment, hippocampal tissues were harvested and processed for Western blot analysis of autophagy-related markers, including LC3-I/II and p62/SQSTM1. Autophagic flux was evaluated by comparing LC3-II accumulation in chloroquine-treated and untreated animals. An increase in LC3-II levels following chloroquine administration was interpreted as evidence of ongoing autophagic flux, whereas a lack of further LC3-II accumulation was considered indicative of impaired autophagic degradation. Changes in p62/SQSTM1 expression were assessed as a complementary marker of autophagic activity.

Behavioral assessments

The behavioral testing was carried during the light phase (09:00-15:00 h) in a temperature controlled, sound muted room, where the experimenter was blinded to group assignments. The mice were first acclimatized to the testing environment before experimentation and the apparatuses were washed with 70 % ethanol between trials to remove olfactory cues.

Morris water maze (MWM)

The Morris water maze was used to measure spatial learning and memory. The device was made of a circular pool (120 cm diameter) of opaque water held at 22±1 °C. An escape platform (10 cm diameter) was placed 1 cm under the surface of the water in a predetermined target quadrant. Mice were trained during 5 days (four trials/day; trial limit of 60 s). An automated video tracking system was used to measure escape latency. A probe trial was established 24 h following the last training session, during which the platform was removed and the percentage of time spent in the target quadrant was used as an index of spatial memory retention. Swimming speed was recorded to control for age-related motor differences.

Novel object recognition (NOR) test

The novel object recognition test was used to measure recognition memory. Mice were conditioned to an open-field arena (40×40×40 cm) during 10 min/day in two days. The two objects were taken for 10 min during the training phase. Following 24 h retention interval, a familiar object was substituted with a new object, and mice were left to explore during 10 min. The time of exploration was documented and recognition memory was expressed as a discrimination index as (T_novel − T_familiar)/(T_novel + T_familiar).

Tissue collection and brain dissection

After behavioral tests were carried out, mice were anesthetized deeply by means of intraperitoneal injection of ketamine (100 mg/kg) and xylazine (10 mg/kg) until full reflex loss. Transcardial perfusion of the animals with ice-cold phosphate-buffered saline (PBS; 0.01 M, pH 7.4) was then carried out to eliminate the circulating blood and reduce postmortem oxidative and proteolytic alterations. Perfusion was done through the left ventricle at a fixed flow rate (approximately 10 ml/min) until the effluent from the right atria was clear to provide an effective clearance of the blood vessels.

Brains were quickly removed and placed on an ice-chilled dissection stage immediately after the perfusion. The cerebral hemispheres were then dissected using fine microdissection tools and using anatomical landmarks to ensure that the hippocampus was thoroughly dissected on ice to maintain the integrity of proteins and redox sensitive molecular markers. Special attention was paid to mechanical damage and cross-contamination between brain regions.

Tissues that were to undergo biochemical and molecular studies (Western blotting, oxidative stress assays, and mitochondrial measurements) were snap-frozen in liquid nitrogen to stop the activity of the enzymes and to prevent oxidation after extraction. The frozen samples were kept at -80 °C until further use. All samples were processed within a short time window in order to reduce variability.

Whole brains were post-fixed in 4 % paraformaldehyde (PFA) in PBS (pH 7.4) at 4 °C overnight. After fixation, the brains were thoroughly washed using PBS and cryoprotected by immersing in the 15 % and then 30 % solutions of sucrose in the PBS successively until the tissues sank, indicating full cryoprotection. Embedding of cryoprotected brains was done in optimal cutting temperature (OCT) compound and kept at -80 °C until sectioning.

Coronal sections of the brain (30 µm thick) of the hippocampal areas were acquired by the cryostat at -20 °C. A series of sections were collected to provide anatomical consistency between animals and stored in cryoprotectant solution at -20 °C until immuno-histochemical treatment.

Western blot analysis

Protein extraction

Radioimmunoprecipitation assay (RIPA) buffer containing 50 mM tris-HCl (pH 7.4), 150 mM NaCl, 1%

NP-40, 0.5 % sodium deoxycholate and 0.1 % SDS was used to homogenize frozen hippocampal tissue on ice in the presence of a complete protease inhibitor cocktail and phosphatase inhibitors (1 mM sodium orthovanadate, 10 mM sodium fluoride). A motorized homogenizer (15-20 strokes) was used to homogenize it. Lysates were kept on ice and gently swirled and centrifuged at 14,000× g at 4 °C in 20 min. The supernatants were gathered, aliquoted and kept at -80 °C pending utilization.

Protein quantification

The concentration of total protein was measured by bicinchoninic acid (BCA) assay and bovine serum albumin was taken as a standard. All the samples were adjusted to equal protein concentrations before being subjecting to electrophoresis.

SDS-PAGE

The proteins were loaded with equal quantities of protein (30-40 µg per lane) combined with 4× Laemmli sample buffer with 5 % β-mercaptoethanol and subjected to 95 °C heating for 5 min. The proteins were separated on 10-15 % SDS-polyacrylamide gels with 5 % β-mercaptoethanol depending on the molecular weight of the proteins of interest (15 % of LC3, 10-12 % of GPX4, ACSL4). After the electrophoresis, proteins were moved onto polyvinylidene difluoride (PVDF) membranes that were pre-activated in methanol through wet transfer system at 100 V in 90 min at 4 °C.

Membrane blocking and antibody incubation

Depending on the antibody needs, the membranes were blocked 1 h at room temperature in 5 % non-fat dry milk or 5 % bovine serum albumin (BSA) in Tris-buffered saline with 0.1 % Tween-20 (TBST). Primary antibodies were incubated overnight on membranes. Primary antibodies were: anti-GPX4 (1:1000), anti-SLC7A11 (1:1000), anti-ACSL4 (1:1000), anti-LC3B (1:1000), anti-beclin-1 (1:1000), anti-p62/SQSTM1 (1:1000), anti-LC3-I/II (1:2000), anti-P62 (1:1000), anti-PSD95 (1:1000), anti-Synaptophysin (1:2000) and anti-β-actin (1:5000). Primary incubation was followed by three washes of the membranes (10 min each) in TBST, and incubation on horseradish peroxidase (HRP)-conjugated species-specific secondary antibodies (1:5000) (1 h at room temperature).

Detection and quantification

The immunoreactive bands were developed with the help of enhanced chemiluminescence (ECL) reagents and visualized with a digital imaging system. The exposure times were also optimized in order to prevent saturation of signals. ImageJ software was used to quantify the band intensities and normalize the protein expression levels to β-actin. In the case of LC3, the ratio of LC3-II to LC3-I was determined as an index of autophagosome formation, while autophagic flux was assessed by evaluating LC3-II accumulation following chloroquine treatment.

Lipid peroxidation measurements

MDA assay

The level of lipid peroxidation was measured by measuring malondialdehyde (MDA) through the thiobarbituric acid reactive substances (TBARS) assay. Homogenates of tissues were added to TBA reagent and kept at 95 °C for 60 min. Samples were cooled and centrifuged at 10,000× g during 10 min and absorbance was taken at 532 nm. Standard curve with 1,1,3,3-tetra-methoxypropane was used to determine the MDA concentrations which were then expressed as nmol/mg of protein.

4-HNE ELISA

The amount of ELISA kit, 4-HNE-protein adducts was measured as per the instructions given in the commercially available ELISA kit (Elabscience, catalog No: E-EL-0128). At 450 nm, the absorbance was obtained and the concentrations were adjusted to total protein content.

Mitochondrial isolation and redox analyses

Mitochondrial isolation

A differential centrifugation protocol was used to isolate mitochondria with intact integrity from freshly dissected hippocampal tissue. All procedures were performed at 4 °C to reduce proteolysis and oxidative damage. Tissues samples were homogenized in ice-cold mitochondrial isolation buffer containing 225 mM mannitol, 75 mM sucrose, 5 mM HEPES and 1 mM EGTA (pH 7.4) with protease inhibitors.

A glass-Teflon homogenizer was used with 10-12 light strokes. Centrifugation was performed at 800× g for 10 min to remove nuclei and debris. The supernatant was centrifuged at 10,000× g for 15 min to pellet crude mitochondria. The pellet was washed once and centrifuged again at 10,000× g for 10 min. The mitochondrial pellet was resuspended in isolation buffer

and protein concentration was measured using BCA assay. ROS measurements were performed immediately.

Detection of mitochondrial reactive oxygen species (ROS)

Mitochondrial ROS was quantified using 2',7'-dichlorofluorescein diacetate (DCF-DA) fluorescence assay. Isolated mitochondria (50 µg protein) were incubated with 10 µM DCF-DA at 37 °C and in the dark for 30 min. Fluorescence was measured at excitation/emission wavelengths at 485/530 nm. Background fluorescence was subtracted and ROS levels were expressed as relative fluorescence units per mg protein.

Total antioxidant capacity assay

Total antioxidant capacity was measured using the ferric reducing antioxidant power (FRAP) assay. Samples were combined with freshly prepared FRAP reagent (acetate buffer, TPTZ, ferric chloride). The reaction mixture was incubated 37 °C for 30 min. Absorbance was measured at 593 nm using a spectrophotometer. A ferrous sulfate standard curve was used to obtain antioxidant capacity which was presented as µmol Fe^{2+} equivalents per mg protein.

SOD2 and HO-1 ELISA

Quantification of the levels of SOD2 and HO-1 was performed by using a commercially available ELISA kit following manufacturer's instructions. Homogenates of the brains were prepared and centrifuged in ice-cold lysis buffer to remove debris. An equal amount of protein from each sample was loaded into ELISA plates that had been pre-coated with specific antibodies against SOD2 or HO-1. Incubation and washing were then performed, followed by addition of horseradish peroxidase (HRP)-conjugated secondary antibodies and substrate solution. Stop solution was used to stop the colorimetric reaction and absorbance was observed at 450 nm using a microplate reader. Standard curves were used to determine concentrations of SOD2 and HO-1 based on protein content.

Histopathological analysis

After behavioral tests, the mice were deeply anesthetized and transcardially perfused with ice-cold phosphate-buffered saline (PBS) and 4 % paraformaldehyde (PFA) in PBS. Brains were excised and fixed 4 % PFA at 4 °C for 24 h, followed by dehydration using a graded series of ethanol (70 %, 80 %, 95 % and 100 %), cleared using xylene, and embedded in paraffin.

Coronal sections of the brain (5 µm thickness) were cut using a rotary microtome, mounted on gelatin-coated slides and allowed to dry overnight at 37 °C. Sections were then deparaffinized using xylene, rehydrated using progressive concentrations of ethanol, and washed with distilled water.

In general, histopathological examination and hematoxylin and eosin (H&E) staining were performed according to routine procedures. In brief, the sections were stained with hematoxylin to visualize nuclei, rinsed in tap water, differentiated in 1 % acid alcohol where required, blued in alkaline solution and counterstained with eosin. The sections were dried using graded alcohols, cleaned in xylene and mounted with permanent mounting medium.

The histological examination was performed using a light microscope. Respective images of hippocampal areas were taken at the same magnification and exposure parameters in all groups. Neuronal morphology, cellular density and tissue structure were measured and the histopathological changes (neuronal loss, vacuolation and pyknosis) were analyzed using ImageJ software in anatomically equivalent regions.

Statistical analysis

All the experiments were performed on biological replicates, and biochemicals were done in technical triplicates. The data are presented as mean ± SEM. To determine the effects of age and treatment, two-way ANOVA was performed, followed by appropriate *post hoc* tests for multiple comparisons. Two-way repeated-measures ANOVA was used to analyze Morris water maze training data. The level of statistical significance was fixed at $p<0.05$. GraphPad Prism was used for statistical analysis and data visualization.

Results

Artesunate enhances cognitive function in STZ-induced AD in age-dependent manner

Spatial learning and memory were used as measures of the effects of artesunate on cognitive impairments caused by STZ, the Morris water maze (MWM) was used to test spatial learning and memory in young and old mice, whereas recognition memory was tested using the novel object recognition (NOR) test.

The STZ-treated young and old mice at the

acquisition stage of the MWM displayed a noticeable increase in escape latency across training days relative to their respective age-matched controls, indicating impaired spatial learning. The treatment of the young STZ mice with artesunate significantly decreased the escape latency and the performance gradually approached control levels by day 5 compared with the STZ group. Conversely, the performance of old STZ mice treated with artesunate was only slightly improved, with escape latencies remaining considerably higher relative to controls.

During the probe trial, the young STZ mice took much less time in the target quadrant than controls, which confirms impaired spatial memory. Artesunate was found to considerably increase target quadrant occupancy in young STZ mice, but only partially and non-significantly improved target quadrant occupancy in old STZ mice. There were no significant differences in swim speed between groups, ruling out motor impairment as a confounding factor.

In line with MWM results, a significant change in discrimination index was found in STZ-treated mice of the two age categories in NOR testing. Artesunate strongly reinstated recognition memory in young STZ mice, whereas old STZ displayed only slight recovery, remaining significantly impaired compared with age-matched controls.

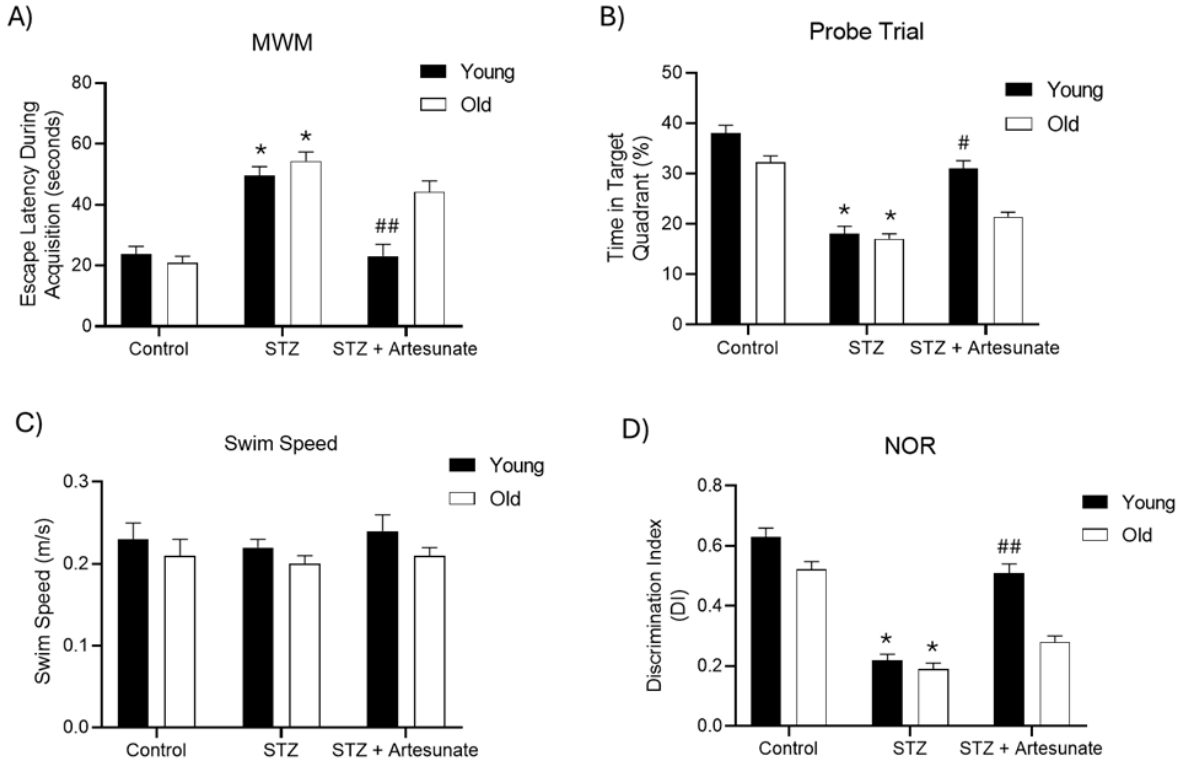


Fig. 1. Artesunate enhances learning and memory in young but not old STZ induced AD mice. (**A**) Morris water maze (MWM) training with escape latency during five days. (**B**) proportion of time in target quadrant at probe trial. (**C**) Swim speed test which evaluates locomotor activity. (**D**) Discrimination index of familiar object recognition (NOR) test. Data are presented as mean ± SEM; n=10 mice per group. Statistical analysis was performed using two-way ANOVA (MWM training) and one-way ANOVA followed by Tukey's *post hoc* test for other comparisons. * $p<0.05$ vs. control group, # $p<0.05$; ## $p<0.01$ vs. STZ group (young).

Artesunate inhibits ferroptotic signaling predominantly in young AD brains

To find out whether artesunate is age-dependently modulating ferroptosis, the level of major ferroptotic regulators, such as GPX4, SLC7A11, and ACSL4, was examined through Western blotting in hippocampal tissues.

STZ treatment led to a significant decrease in GPX4 and SLC7A11 expression and a subsequent increase in ACSL4 expression in young and old mice, which is evidence of the activation of ferroptotic pathways. Treatment with artesunate significantly restored GPX4 and SLC7A11 expression and suppressed ACSL4 expression in young STZ mice. Old STZ mice, on the other hand, showed partial GPX4 and SLC7A11 restoration, whereas ACSL4 levels remained significantly elevated compared with controls.

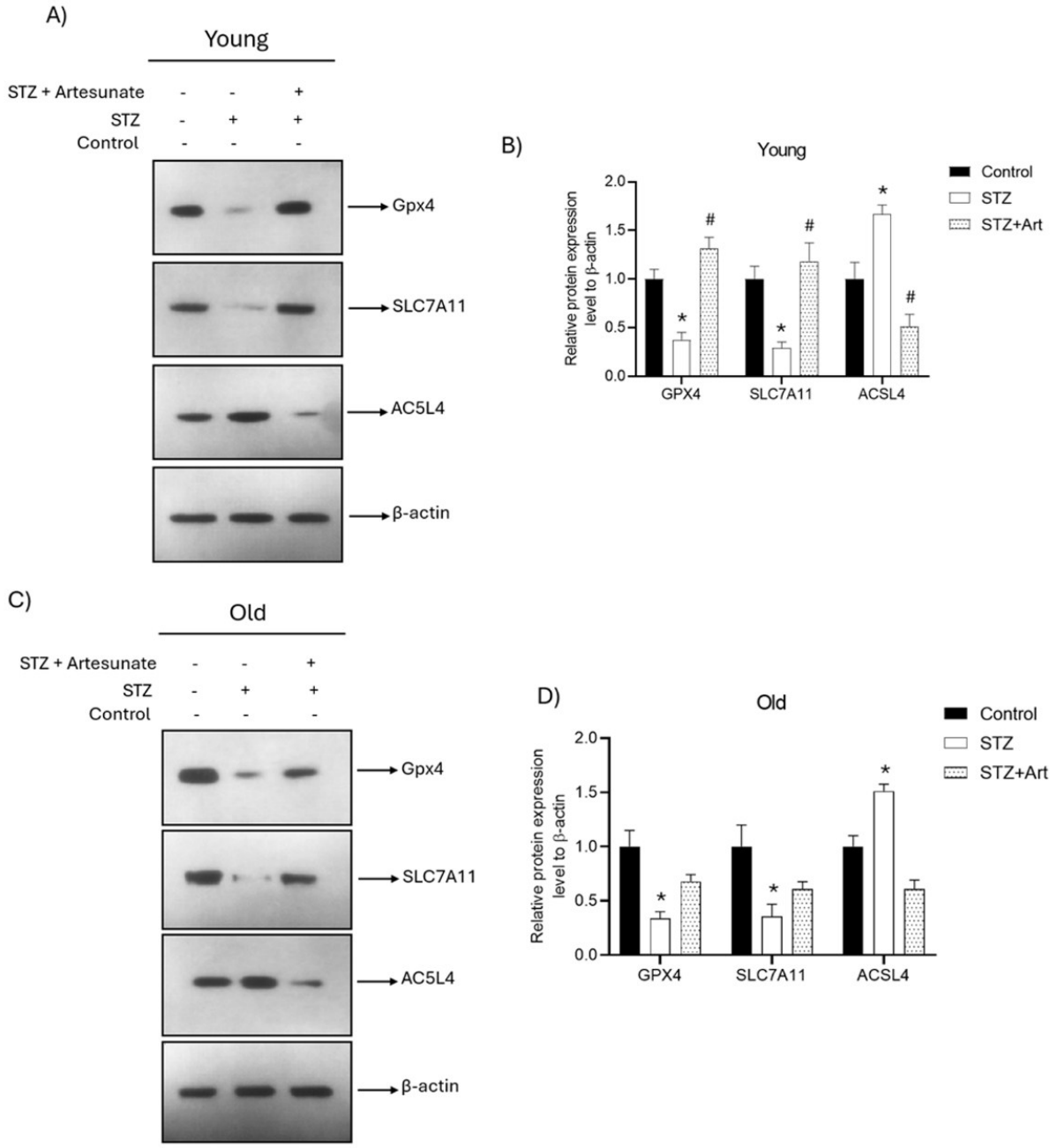


Fig. 2. Artesunate selectively deals with ferroptosis-related proteins in young and old AD brains. (**A**) Protein expression levels of GPX4, SLC7A11, and ACSL4 in the hippocampal tissues of young mice shown by representative Western blots. (**B**) Densitometric analysis of GPX4, SLC7A11, and ACSL4 protein levels in young mice. (**C**) Protein expression levels of GPX4, SLC7A11, and ACSL4 in the hippocampal tissues of old mice shown by representative Western blots. (**D**) Densitometric analysis of GPX4, SLC7A11, and ACSL4 protein levels in old mice. Densitometric data are presented as mean ± SEM; n=5 mice per group. Statistical analysis was performed using one-way ANOVA followed by Tukey's *post hoc* test. * $p<0.05$ vs. control group, # $p<0.05$ vs. STZ group (young).

Artesunate inhibits lipid peroxidation more effectively in young mice than old mice

Since lipid peroxidation is a key event in ferroptosis, the concentration of malondialdehyde (MDA) and 4-hydroxynonenal (4-HNE) were measured.

The level of MDA and 4-HNE were highly elevated by STZ in both age groups, indicating widespread lipid peroxidation. Artesunate therapy had a strong effect on the reduction of MDA and 4-HNE levels in young STZ mice, returning the levels to near control. Nevertheless, artesunate was not able to completely prevent lipid peroxidation in old STZ mice, and the levels of MDA and 4-HNE were still high compared to the control. These results show that aging reduces the effectiveness of artesunate in suppressing ferroptosis-associated lipid peroxidation.

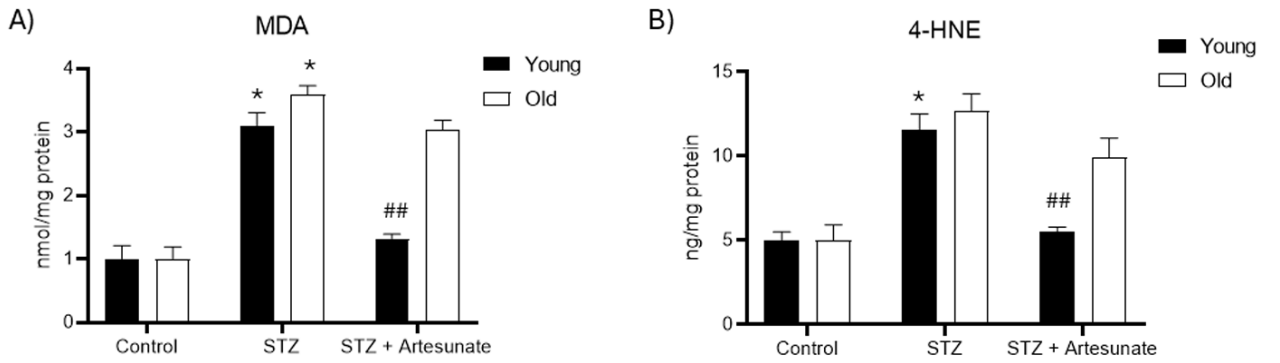


Fig. 3. Artesunate inhibits the lipid peroxidation in younger compared to older mice. (**A**) Levels of MDA in the hippocampal tissues of young and old mice (**B**) Levels of 4-HNE in the hippocampal tissues of young and old mice. Data are presented as mean ± SEM; n=6 mice per group. Statistical analysis was performed using one-way ANOVA followed by Tukey's *post hoc* test. * p<0.05 vs. control group, ## p<0.01 vs. STZ group (young).

Artesunate partially recovers autophagic flux age-dependent recovery

The evaluation of autophagic activity was based on the conversion of LC3-I/II, Beclin-1, and p62. STZ therapy had a significant negative effect on the LC3-II/LC3-I ratio and Beclin-1 expression and a positive effect on p62 accumulation in young and old mice which is a sign of impaired autophagic flux.

Artesunate greatly enhanced LC3-II and Beclin-1 expression and decreased p62 accumulation in young STZ mice. LC3-II accumulation was also further increased by pretreatment with chloroquine, which is a further indication of intact autophagic flux. Old STZ mice, on the other hand, were only partially normalized in both LC3-II and Beclin-1, with p62 levels remaining high, indicating partial recovery of autophagy.

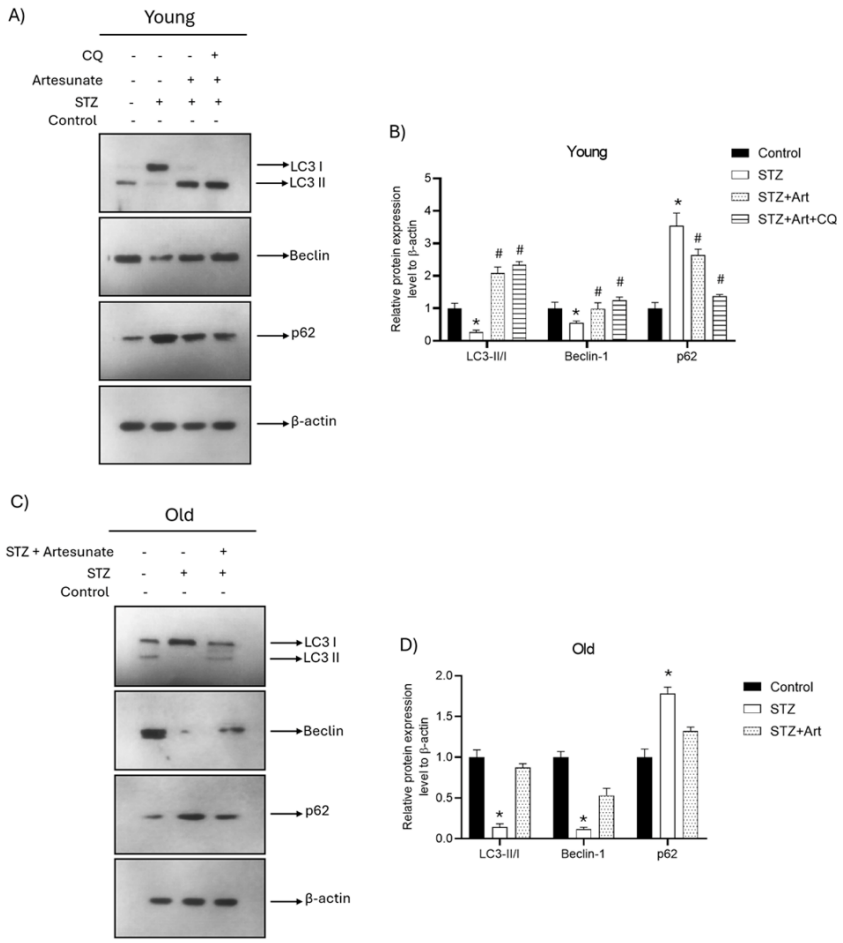


Fig. 4. Artesunate partially restores age-dependent autophagic flux. (**A**) Protein expression levels of LC3-I/II, Beclin-1, and p62 in the hippocampal tissues of young mice shown by representative Western blots. (**B**) Densitometric analysis of LC3-I/II, Beclin-1, and p62 protein levels in young mice. (**C**) Protein expression levels of LC3-I/II, Beclin-1, and p62 in the hippocampal tissues of old mice shown by representative Western blots. (**D**) Densitometric analysis of LC3-I/II, Beclin-1, and p62 protein levels in old mice. Densitometric data are presented as mean ± SEM; n=5 mice per group. Statistical analysis was performed using one-way ANOVA followed by Tukey's *post hoc* test. * p<0.05 vs. control group, and # p<0.01 vs. STZ + Art group.

Artesunate restores mitochondrial redox homeostasis in young mice preferentially

Mitochondrial oxidative stress was evaluated based on the production of mitochondrial ROS, the expression of antioxidant enzymes (SOD2 and HO-1), or total antioxidant capacity.

STZ was found to induce a considerable increase in the production of mitochondrial ROS and a decrease in SOD2, HO-1 and FRAP values in both age groups. Mitochondrial ROS was substantially inhibited and antioxidant defenses in young STZ mice were restored by artesunate treatment. Conversely, old STZ mice were characterized by the persistent increase of mitochondrial ROS and minimal restoration of antioxidant enzyme expression. These data point to the fact that aging worsens the ability of artesunate restore mitochondrial redox homeostasis.

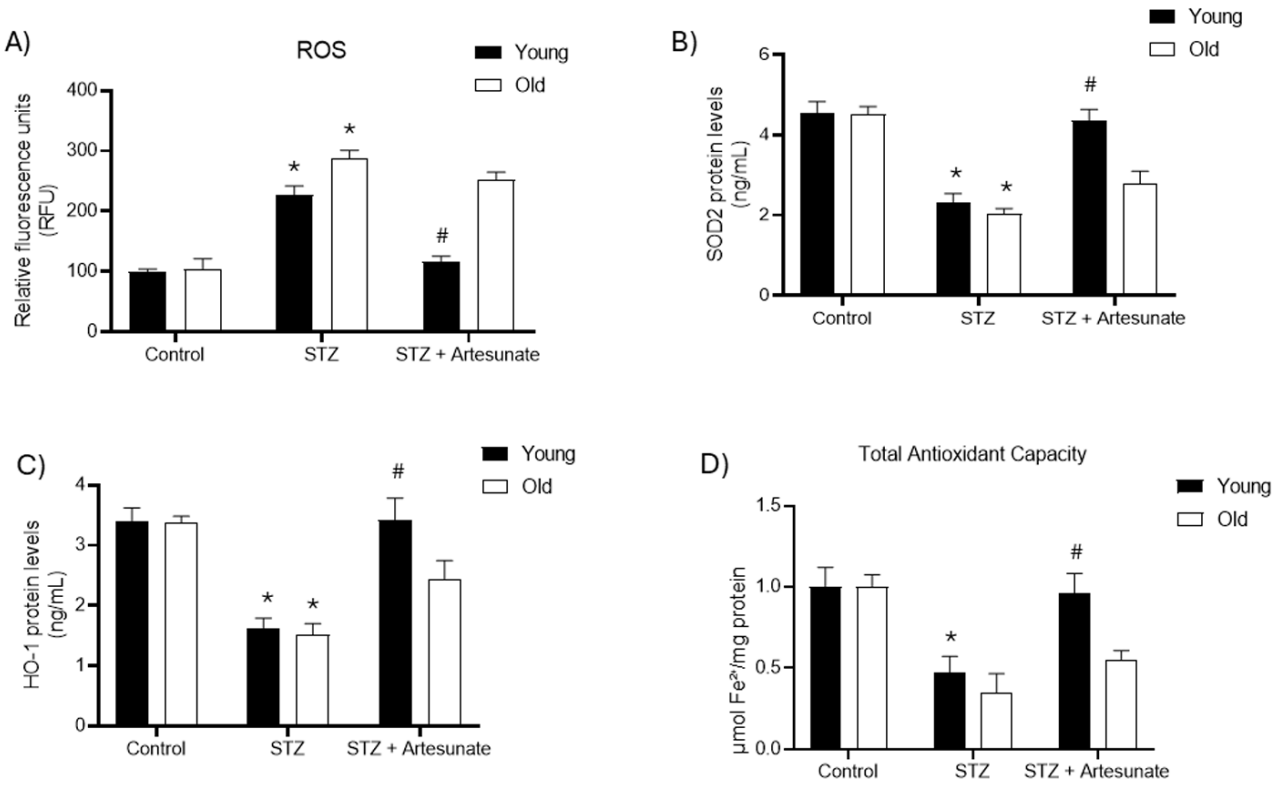


Fig. 5. Artesunate is selective in mitochondrial restoring redox balance preferentially in young mice. (**A**) Mitochondrial ROS levels in the hippocampal tissues of young and old mice. (**B**) Levels of SOD2 in the hippocampal tissues of young and old mice. (**C**) Levels of HO-1 in the hippocampal tissues of young and old mice. (**D**) Total antioxidant capacity in the hippocampal tissues of young and old mice. Data are presented as mean ± SEM; n=6 mice per group. Statistical analysis was performed using one-way ANOVA followed by Tukey's *post hoc* test. * $p<0.05$ vs. control group, and # $p<0.01$ vs. STZ group (young).

Artesunate preserves synaptic integrity and suppresses histopathological changes in young but not old ad mice

The integrity of synapses was assessed through quantifying the expression of PSD95 and synaptophysin, which are key markers of postsynaptic and presynaptic integrity. The levels of PSD95 and synaptophysin were also lessened considerably by STZ treatment in both age groups. Artesunate significantly recovered synaptic protein levels in young STZ mice, but old STZ mice had small, but non-significant recovery, consistent with persistent impairment of cognitive function.

H&E staining showed significant loss of neurons, cytoplasmic vacuolation and pyknotic nuclei in hippocampus in STZ treated mice. Artesunate significantly enhanced the morphology of neurons and decreased degenerative characteristics of young STZ mice, but old mice still exhibited a high degree of histopathological abnormalities. Quantitative analysis showed a significant reduction in neuronal loss in young but not old mice.

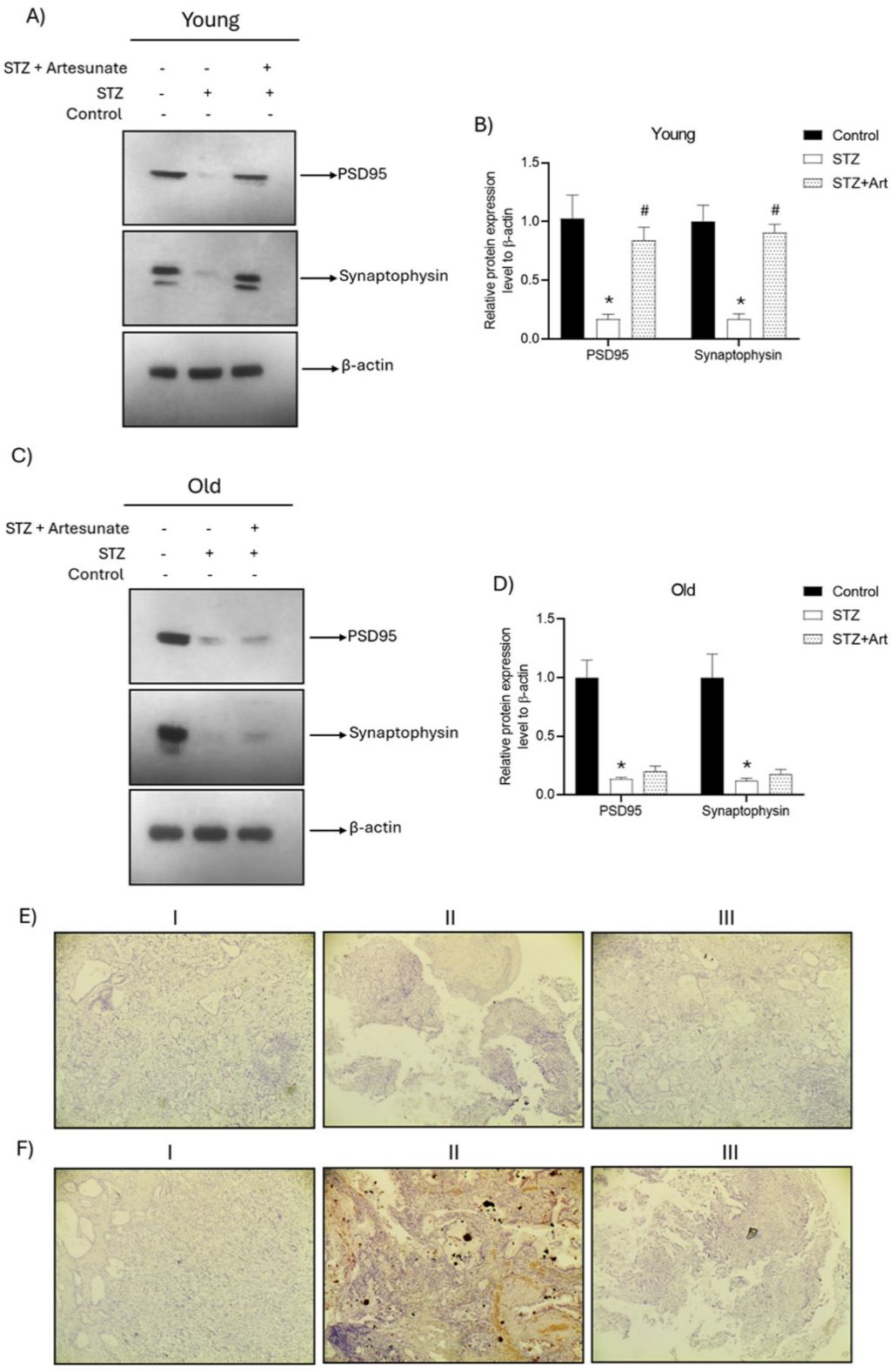


Fig. 6. Artesunate restores synaptic integrity and suppresses histopathological changes in young and not old AD mice. (**A**) Representative Western blots showing expression levels of PSD95 and synaptophysin proteins in the hippocampal tissues of young mice. (**B**) Densitometric analysis of PSD95 and synaptophysin protein levels in young mice. (**C**) Representative Western blots showing expression levels of PSD95 and synaptophysin proteins in the hippocampal tissues of old mice. (**D**) Densitometric analysis of PSD95 and synaptophysin protein levels in old mice. (**E**) Representative hematoxylin and eosin (H&E)-stained hippocampal sections with (I) normal histology, (II) STZ group, (III) STZ + artesunate group in the young mice. (**F**) Representative H&E-stained hippocampal sections with (I) normal histology, (II) STZ group, (III) STZ + artesunate group in the old mice. Scale bar = 100 μm. Data are presented as mean ± SEM; n=5 mice per group. Statistical analysis was performed using one-way ANOVA followed by Tukey's *post hoc* test. * $p<0.05$ vs. control group, and # $p<0.01$ vs. STZ group (young).

Discussion

The current paper shows that artesunate has a strong yet age-related neuroprotective property in streptozotocin (STZ)-induced model of intermittent Alzheimer-like pathology. Our results indicate that artesunate selectively maintains cognitive, synaptic, and redox homeostasis in young mice, but not in the aged, by combining behavioral, molecular, biochemical, mitochondrial, and histopathological studies. These findings are in line with a great deal of published evidence that ferroptosis, dysfunctional autophagy, and mitochondrial oxidative stress are mutually reinforcing mediators of Alzheimer's disease (AD) pathology and mechanisms that become less responsive to therapeutic regulation with age [27].

Importantly, baseline comparisons between age-matched control groups revealed that aged control mice already exhibited significantly impaired cognitive performance and reduced synaptic, mitochondrial antioxidant, and autophagic markers compared with young controls, consistent with physiological brain aging. This confirms that aging itself contributes to a pre-existing decline in neuronal resilience, which likely influences the differential responsiveness to artesunate observed in this study.

The STZ-induced cognitive impairment in young and old mice is consistent with the previous research showing that intracerebroventricular STZ causes brain insulin resistance, mitochondrial dysfunction, oxidative stress and synaptic loss similar to sporadic AD [28]. It has been demonstrated by many reports that STZ interferes with hippocampal-dependent spatial learning and recognition memory, which is mediated by lipid peroxidation and mitochondrial dysfunction, which is increased in aged brains [29]. The present study showed that artesunate significantly enhanced spatial learning and recognition memory in young STZ-treated mice, but showed only minimal behavioral recovery in old animals. Age-dependent differences of antioxidants and autophagy-modulating agents in experimental models of AD have been reported, which supports the idea that aging restricts the effects of treatment by restricting molecular flexibility and neuronal plasticity.

Ferroptosis is emerging as a major cause of neurodegeneration in AD, and human postmortem and animal models show decreased GPX4 activity, defective cystine uptake by SLC7A11, and increased ACSL4-mediated lipid remodelling [30]. In line with these results, the administration of STZ in the current experiment led to the downregulation of GPX4 and SLC7A11 and upregulation of ACSL4 in young and old mice, which revealed the activation of ferroptotic pathways. Artesunate was able to reestablish GPX4 and SLC7A11 expression and inhibit ACSL4 upregulation in young mice, consistent with prior reports indicating that artesunate regulates ferroptosis by maintaining glutathione-dependent antioxidant defenses and preventing iron-mediated lipid peroxidation. On the contrary, the partial normalization of ferroptosis-related proteins in old mice is in line with the existing literature that identifies that aging correlates with a decrease in GPX4 levels, alterations in iron homeostasis, and enhanced sensitivity to ferroptotic injury, which leads to a lack of responses to ferroptosis-targeted therapies [31].

Lipid peroxidation is a hallmark pathological characteristic of AD and an occurrence in ferroptosis [32]. The increased levels of malondialdehyde (MDA) and 4-hydroxynonenal (4-HNE) have been found in AD patients and in the experimental models, which are associated with synaptic dysfunction and neuronal loss [33]. Consistent with these reports, the level of MDA and 4-HNE was significantly elevated in the two age groups with STZ treatment. Artesunate was able to substantially decrease lipid peroxidation in young mice but aged mice had continued and increased MDA and 4-HNE regardless of treatment. These results are reinforced by previous research that revealed that aging is linked to lipid oxidation, loss of lipid aldehyde detoxification, and decline in the ability to repair lipid ferro-oxidative damages and ferroptotic signatures of the aged brain [34].

Autophagic dysfunction is one of the hallmarks of AD and is well-established [35]. There is a lower LC3-II formation, lowering of Beclin-1 expression and p62 build-up in AD brains, which further increases with age [36]. The current research supports the fact that STZ disrupts autophagic flux in both young and old mice, which is in agreement with the past data assessing the relationship between insulin resistance and oxidative stress with autophagic dysfunction. Artesunate rescued LC3-II and Beclin-1 expression and decreased p62 accumulation in young mice, and this shows that autophagic flux was restored, as has been reported to show that artesunate increases autophagy *via* redox-sensitive signaling pathways. Conversely, aged mice showed partial recovery of autophagic markers, which is in line with much of the literature that indicates age-induced impairments in lysosomal functioning and autophagosome clearance, that restrain pharmacological salvaging of autophagy [37].

Early and sustained pathological features of AD are

mitochondrial dysfunction and oxidative stress [38]. Human AD brains and STZ-based models have been shown to have reduced the expression of mitochondrial antioxidant enzymes including SOD2 and HO-1, and increased mitochondrial ROS [39]. These observations are in line with our findings that STZ elevated mitochondrial ROS and inhibited antioxidant defenses in the two age groups. Artesunate had a significant effect on mitochondrial ROS, as well as on the restoration of SOD2 and HO-1 expression in young mice, which agrees with other reports that artesunate promotes redox homeostasis in mitochondria [26]. Nevertheless, elderly mice maintained chronic mitochondrial oxidative stress after treatment, which is in line with the reports that aging impairs mitochondrial resilience, antioxidant induction as well as redox signaling ability [40]. The greatest pathological correlate of cognitive impairment in AD is synaptic loss, and reduced expression of synaptic markers including PSD95 and synaptophysin has been extensively reported in human and experimental AD [41]. The current research has shown that STZ has caused synaptic losses of proteins in young and geriatric mice. Artesunate strongly replenished synaptic protein expression in young mice but not in aged animals. These results align with the evidence that the efficient inhibition of oxidative stress, ferroptosis, and autophagy dysfunction is needed to preserve synapses, and that sustained redox imbalance in the aged brain prevents synaptic restoration [42].

The neuroprotective effects of artesunate were also age-dependent as supported by histopathological analysis. The STZ treated mice had changes of neuronal loss, cytoplasmic vacuolation and nuclear pyknosis as has been previously described in STZ induced neurodegeneration. Artesunate significantly ameliorated neuronal morphology and degenerative characteristics in young mice and aged mice still exhibited significant histopathological alterations. These findings are consistent with the research that indicates that there is little structural restoration in the elderly brains after neuroprotective treatments.

Limitations

This study has several limitations that should be acknowledged. First, the experiments were conducted exclusively in male mice; therefore, potential sex-dependent differences in artesunate responsiveness were not evaluated. Second, direct measurements of brain iron levels were not performed, which limits definitive conclusions regarding iron accumulation and its contribution to ferroptosis modulation. Third, classical Alzheimer's disease-related pathological hallmarks such as amyloid-β and tau phosphorylation were not assessed, which restricts comparison with full-spectrum AD pathology. Fourth, no dose-response analysis of artesunate was conducted, and therefore the optimal therapeutic concentration could not be determined. Finally, although associations between ferroptosis, autophagy, mitochondrial dysfunction, and cognitive outcomes were demonstrated, the study does not establish a direct causal relationship between these pathways and the observed behavioral improvements.

Conclusions

Altogether, the current results indicate that artesunate shows age-dependent neuroprotective effects in STZ-induced Alzheimer-like pathology through the regulation of the ferroptosis-autophagy-mitochondrial redox axis. Although artesunate demonstrated protective effects against ferroptotic alterations, improved autophagy markers, enhanced mitochondrial antioxidant status, and preserved synaptic integrity in young mice, its efficacy was markedly reduced in aged animals, indicating that aging is a major limiting factor for these protective actions.

The findings are in agreement with a growing body of literature suggesting that aging phenomenon subjects' therapeutic responsiveness to molecular constraints in AD, confirming the significance of age-related approaches in the context of redox- and ferroptosis-related pathways targeting in targeting Alzheimer's disease.

Conflict of Interest

There is no conflict of interest.

Acknowledgements

The authors acknowledge the support of their respective institutions for providing the necessary facilities to carry out this research.

References

1. Tenchov R, Sasso JM, Zhou QA. Alzheimer's Disease: Exploring the Landscape of Cognitive Decline. ACS Chem Neurosci 2024;15:3800-3827. https://doi.org/10.1021/acschemneuro.4c00339

2. Zhang H, Wei W, Zhao M, Ma L, Jiang X, Pei H, Cao Y, Li H. Interaction between Abeta and Tau in the Pathogenesis of Alzheimer's Disease. Int J Biol Sci 2021;17:2181-2192. https://doi.org/10.7150/ijbs.57078
3. Wang W, Zhao F, Ma X, Perry G, Zhu X. Mitochondria dysfunction in the pathogenesis of Alzheimer's disease: recent advances. Mol Neurodegener 2020;15:30. https://doi.org/10.1186/s13024-020-00376-6
4. Rummel NG, Butterfield DA. Altered Metabolism in Alzheimer Disease Brain: Role of Oxidative Stress. Antioxid Redox Signal 2022;36:1289-1305. https://doi.org/10.1089/ars.2021.0177
5. Perez Ortiz JM, Swerdlow RH. Mitochondrial dysfunction in Alzheimer's disease: Role in pathogenesis and novel therapeutic opportunities. Br J Pharmacol 2019;176:3489-3507. https://doi.org/10.1111/bph.14585
6. Kowalczyk P, Sulejczak D, Kleczkowska P, Bukowska-Osko I, Kucia M, Popiel M, et al. Mitochondrial Oxidative Stress-A Causative Factor and Therapeutic Target in Many Diseases. Int J Mol Sci 2021;22:13384. https://doi.org/10.3390/ijms222413384
7. Kim S, Jung UJ, Kim SR. Role of Oxidative Stress in Blood-Brain Barrier Disruption and Neurodegenerative Diseases. Antioxidants (Basel) 2024;13:1462. https://doi.org/10.3390/antiox13121462
8. Zhang X, Gao Y, Zhang S, Wang Y, Pei X, Chen Y, et al. Mitochondrial dysfunction in the regulation of aging and aging-related diseases. Cell Commun Signal 2025;23:290. https://doi.org/10.1186/s12964-025-02308-7
9. Ma H, Dong Y, Chu Y, Guo Y, Li L. The mechanisms of ferroptosis and its role in Alzheimer's disease. Front Mol Biosci 2022;9:965064. https://doi.org/10.3389/fmolb.2022.965064
10. Chen F, Kang R, Tang D, Liu J. Ferroptosis: principles and significance in health and disease. J Hematol Oncol 2024;17:41. https://doi.org/10.1186/s13045-024-01564-3
11. Zhuo B, Qin C, Deng S, Jiang H, Si S, Tao F, et al. The role of ACSL4 in stroke: mechanisms and potential therapeutic target. Mol Cell Biochem 2025;480:2223-2246. https://doi.org/10.1007/s11010-024-05150-6
12. Chu J, Li J, Sun L, Wei J. The Role of Cellular Defense Systems of Ferroptosis in Parkinson's Disease and Alzheimer's Disease. Int J Mol Sci 2023;24:14108. https://doi.org/10.3390/ijms241814108
13. Hirata Y, Yamada Y, Taguchi S, Kojima R, Masumoto H, Kimura S, et al. Conjugated fatty acids drive ferroptosis through chaperone-mediated autophagic degradation of GPX4 by targeting mitochondria. Cell Death Dis 2024;15:884. https://doi.org/10.1038/s41419-024-07237-w
14. Xie Y, Kang R, Klionsky DJ, Tang D. GPX4 in cell death, autophagy, and disease. Autophagy 2023;19:2621-2638. https://doi.org/10.1080/15548627.2023.2218764
15. Khan G, Hussain MS, Khan Y, Fatima R, Ahmad S, Sultana A, Alam P. Ferroptosis and its contribution to cognitive impairment in Alzheimer's disease: mechanisms and therapeutic potential. Brain Res 2025;1864:149776. https://doi.org/10.1016/j.brainres.2025.149776
16. Gomez-Virgilio L, Silva-Lucero MD, Flores-Morelos DS, Gallardo-Nieto J, Lopez-Toledo G, Abarca-Fernandez AM, et al. Autophagy: A Key Regulator of Homeostasis and Disease: An Overview of Molecular Mechanisms and Modulators. Cells 2022;11:2262. https://doi.org/10.3390/cells11152262
17. Cai Q, Jeong YY. Mitophagy in Alzheimer's Disease and Other Age-Related Neurodegenerative Diseases. Cells 2020;9:150. https://doi.org/10.3390/cells9010150
18. Kang R, Tang D. Autophagy and Ferroptosis - What's the Connection? Curr Pathobiol Rep 2017;5:153-159. https://doi.org/10.1007/s40139-017-0139-5
19. Liu MZ, Kong N, Zhang GY, Xu Q, Xu Y, Ke P, Liu C. The critical role of ferritinophagy in human disease. Front Pharmacol 2022;13:933732. https://doi.org/10.3389/fphar.2022.933732
20. Liu X, Luo Q, Zhao Y, Ren P, Jin Y, Zhou J. The Ferroptosis-Mitochondrial Axis in Depression: Unraveling the Feedforward Loop of Oxidative Stress, Metabolic Homeostasis Dysregulation, and Neuroinflammation. Antioxidants (Basel) 2025;14:613. https://doi.org/10.3390/antiox14050613
21. Park J, Won J, Seo J, Yeo HG, Kim K, Kim YG, et al. Streptozotocin Induces Alzheimer's Disease-Like Pathology in Hippocampal Neuronal Cells via CDK5/Drp1-Mediated Mitochondrial Fragmentation. Front Cell Neurosci 2020;14:235. https://doi.org/10.3389/fncel.2020.00235
22. Kaur D, Grewal AK, Almasoudi SH, Almehmadi AH, Alsfouk BA, Kumar A, et al. Neuroprotective effect of Tozasertib in Streptozotocin-induced Alzheimer's mice model. Sci Rep 2025;15:28963. https://doi.org/10.1038/s41598-025-13920-5

23. Okorji UP, Olajide OA. A semi-synthetic derivative of artemisinin, artesunate inhibits prostaglandin E2 production in LPS/IFNγ-activated BV2 microglia. Bioorg Med Chem 2014;22:4726-4734. https://doi.org/10.1016/j.bmc.2014.07.007
24. Zuo S, Li Q, Liu X, Feng H, Chen Y. The Potential Therapeutic Effects of Artesunate on Stroke and Other Central Nervous System Diseases. Biomed Res Int 2016;2016:1489050. https://doi.org/10.1155/2016/1489050
25. Liang L, Liu Y, Wu X, Chen Y. Artesunate induces ferroptosis by inhibiting the nuclear localization of SREBP2 in myeloma cells. Int J Med Sci 2023;20:1535-1550. https://doi.org/10.7150/ijms.86409
26. Zhang J, Sun X, Wang L, Wong YK, Lee YM, Zhou C, et al. Artesunate-induced mitophagy alters cellular redox status. Redox Biol 2018;19:263-273. https://doi.org/10.1016/j.redox.2018.07.025
27. Zhou B, Li J, Wu A, Wang X, Cheng L, Yang G, et al. Insights into targeted ferroptosis in mechanisms, biology, and role of Alzheimer's disease: an update. Front Aging Neurosci 2025;17:1587986. https://doi.org/10.3389/fnagi.2025.1587986
28. Grieb P. Intracerebroventricular Streptozotocin Injections as a Model of Alzheimer's Disease: in Search of a Relevant Mechanism. Mol Neurobiol 2016;53:1741-1752. https://doi.org/10.1007/s12035-015-9132-3
29. Lu Y, Dong Y, Tucker D, Wang R, Ahmed ME, Brann D, Zhang Q. Treadmill Exercise Exerts Neuroprotection and Regulates Microglial Polarization and Oxidative Stress in a Streptozotocin-Induced Rat Model of Sporadic Alzheimer's Disease. J Alzheimers Dis 2017;56:1469-1484. https://doi.org/10.3233/JAD-160869
30. Lane DJR, Metselaar B, Greenough M, Bush AI, Ayton SJ. Ferroptosis and NRF2: an emerging battlefield in the neurodegeneration of Alzheimer's disease. Essays Biochem 2021;65:925-940. https://doi.org/10.1042/EBC20210017
31. Zhang W, Liu Y, Liao Y, Zhu C, Zou Z. GPX4, ferroptosis, and diseases. Biomed Pharmacother 2024;174:116512. https://doi.org/10.1016/j.biopha.2024.116512
32. Chen K, Jiang X, Wu M, Cao X, Bao W, Zhu LQ. Ferroptosis, a Potential Therapeutic Target in Alzheimer's Disease. Front Cell Dev Biol 2021;9:704298. https://doi.org/10.3389/fcell.2021.704298
33. Cecchi C, Fiorillo C, Sorbi S, Latorraca S, Nacmias B, Bagnoli S, et al. Oxidative stress and reduced antioxidant defenses in peripheral cells from familial Alzheimer's patients. Free Radic Biol Med 2002;33:1372-1379. https://doi.org/10.1016/S0891-5849(02)01049-3
34. Hamidu S, Amponsah SK, Aning A, Adams L, Kumi J, Ampem-Danso E, et al. Modulating Ferroptosis in Aging: The Therapeutic Potential of Natural Products. J Aging Res 2025;2025:8832992. https://doi.org/10.1155/jare/8832992
35. Liu J, Li L. Targeting Autophagy for the Treatment of Alzheimer's Disease: Challenges and Opportunities. Front Mol Neurosci 2019;12:203. https://doi.org/10.3389/fnmol.2019.00203
36. Deng M, Huang L, Zhong X. β-asarone modulates Beclin-1, LC3 and p62 expression to attenuate Abeta40 and Abeta42 levels in APP/PS1 transgenic mice with Alzheimer's disease. Mol Med Rep 2020;21:2095-2102. https://doi.org/10.3892/mmr.2020.11026
37. Palmer JE, Wilson N, Son SM, Obrocki P, Wrobel L, Rob M, et al. Autophagy, aging, and age-related neurodegeneration. Neuron 2025;113:29-48. https://doi.org/10.1016/j.neuron.2024.09.015
38. Misrani A, Tabassum S, Yang L. Mitochondrial Dysfunction and Oxidative Stress in Alzheimer's Disease. Front Aging Neurosci 2021;13:617588. https://doi.org/10.3389/fnagi.2021.617588
39. Giorgi C, Marchi S, Simoes ICM, Ren Z, Morciano G, Perrone M, et al. Mitochondria and Reactive Oxygen Species in Aging and Age-Related Diseases. Int Rev Cell Mol Biol 2018;340:209-344. https://doi.org/10.1016/bs.ircmb.2018.05.006
40. Chistiakov DA, Sobenin IA, Revin VV, Orekhov AN, Bobryshev YV. Mitochondrial aging and age-related dysfunction of mitochondria. Biomed Res Int 2014;2014:238463. https://doi.org/10.1155/2014/238463
41. de Wilde MC, Overk CR, Sijben JW, Masliah E. Meta-analysis of synaptic pathology in Alzheimer's disease reveals selective molecular vesicular machinery vulnerability. Alzheimers Dement 2016;12:633-644. https://doi.org/10.1016/j.jalz.2015.12.005
42. Plascencia-Villa G, Perry G. Roles of Oxidative Stress in Synaptic Dysfunction and Neuronal Cell Death in Alzheimer's Disease. Antioxidants (Basel) 2023;12:1628. https://doi.org/10.3390/antiox12081628